Density Segregation of Dry and Wet Granular Mixtures in Gas Fluidized Beds

Stella Lin Li Seah and Eldin Wee Chuan Lim
Dept. of Chemical and Biomolecular Engineering, National University of Singapore, Singapore 117585

DOI 10.1002/aic.14959
Published online August 1, 2015 in Wiley Online Library (wileyonlinelibrary.com)

The Discrete Element Method combined with Computational Fluid Dynamics was coupled to a capillary liquid bridge force model for computational studies of mixing and segregation behaviors in gas fluidized beds containing dry or wet mixtures of granular materials with different densities. The tendency for density segregation decreased with increasing fluidizing velocity, coefficient of restitution, and amount of liquid present. Due to the presence of strong capillary forces between wet particles, there was a high tendency for particles to form agglomerates during the fluidization process, resulting in lower segregation efficiency in comparison with fluidization of dry particles. Particle-particle collision forces were on average stronger than both fluid drag forces and capillary forces. The magnitudes of drag forces and particle-particle collision forces increased with increasing fluidizing velocity and this led to higher mixing or segregation efficiencies observed in dry particles as well as in wet particles at higher fluidizing velocities. © 2015 American Institute of Chemical Engineers *AIChE J*, 61: 4069–4086, 2015

Keywords: mixing and segregation, wet granular materials, fluidized beds, discrete element method, computational fluid dynamics

Introduction

Fluidization is an important multiphase operation in many industrial processes and can be applied for fluid-solid reactions, solids drying, mixing, and various other processes. In many of these operations, fluidization of two or more types of solid particles in a fluidized bed is necessary. Due to differences in sizes, densities and other material properties of the different types of solid particles, the fluidization behavior is expected to be different and much more complex than single-species fluidization. A good understanding of the fluidization and mixing or segregation behaviors of solid particles is instrumental for the design of industrial fluidized bed systems. Although several studies of solids mixing and segregation in fluidized bed systems have been reported in the research literature, mixing or segregation behaviors of wet granular materials during fluidization do not seem to have been adequately addressed to date. Tardos and Pfeffer[1] demonstrated experimentally the occurrence of agglomeration of particles due to the formation of new species during a chemical reaction that occurred on the surface of the particles leading to defluidization. Wright and Raper[2] carried out experiments to investigate the role of liquid bridge forces in fluidization and found that fluidization behavior depended on the liquid bonding between particles and fluidization under low gas velocities strongly depended on the static bridge forces between particles. Rhodes et al.[3] investigated the effects of particle diameter and density on the degree of mixing of uniform particles and observed that particle density had no effect on the equilibrium Lacey index but increasing particle density would increase the rate of mixing. McLaughlin and Rhodes[4] conducted a series of experiments to study the fluidization behavior of a cold model of a gas-solid fluidized bed upon addition of nonvolatile liquids varying in viscosity and surface tension. The wetted particles were observed to stick onto the bed walls and as a result, the weight of particles supported by the gas was lower than the actual weight of the bed. Increasing the amount or viscosity of the liquid changed the fluidization behavior from that of Geldart Group B through A to that of Group C. Wormsbecker and Pugsley[5] conducted experiments to demonstrate the effects of liquid bridging on fluidization behaviors of porous pharmaceutical granules and observed that the granules exhibited Geldart C type fluidization behaviors at high moisture contents and Geldart B type behaviors otherwise. Halow et al.[6] also reported experimental studies of mixing and segregation dynamics of single, magnetically tagged particles in a bubbling fluidized bed. They observed that the spatial distribution of these tracer particles resulting from differences in density was consistent with a Weibull distribution. More recently, Oshitani et al.[7] applied a gas-solid fluidized bed to upgrade iron ore through a density separation process. Nearly perfect separation was achieved and the authors suggested that such continuous density separation processes had the potential to be applied for lump iron ore upgrading. In a subsequent study,[8] simultaneous density and size segregation of particulate iron ore was investigated and it was concluded that an optimum air velocity existed for maximizing segregation.

Apart from experimental studies, wet-particle fluidization behaviors have also been investigated computationally. Cooper and Coronella[9] used an Eulerian-Eulerian approach to

Correspondence concerning this article should be addressed to E. W. C. Lim at chelwce@nus.edu.sg.

simulate a binary fluidized bed and investigate the effects of gas velocity, maximum packing fraction and solids composition on extent of mixing. Huilin et al.[10] investigated fluidization of binary mixtures differing in sizes or densities using an Eulerian-Lagrangian hard-sphere discrete model and reported that an increase in gas velocity resulted in more intense bubble and particle motions, which led to better mixing. The method of coupling Computational Fluid Dynamics with the Discrete Element Method (CFD-DEM) had also been applied extensively in investigations of wet-particle fluidization to extract particle-scale information of the fluidization system. Mikami et al.[11] studied the behavior of a wet powder fluidized bed using CFD-DEM and observed that pressure fluctuations of the wet particle bed were more vigorous than those of the dry particle bed due to accumulation of energy by liquid bridges. Darabi et al.[12] examined the impact of liquid coating on fluidization behavior using a DEM approach and found that more slugs were formed during fluidization when the viscosity or thickness of the liquid coating was increased. More recently, Lim et al.[13] applied the CFD-DEM method coupled with a capillary liquid bridge model to investigate the mixing behaviors of wet particles in a fluidized bed. An analysis of the motion of particles showed unhindered, independent motions for dry particles while wet particles formed agglomerates and exhibited synchronized motions in the form of groups. Apart from fluidized bed systems, a similar approach of coupling DEM with a capillary force model had also been applied for studies of particle mixing[14] and particle segregation[15] due to differences in density and size in rotating drum systems and pattern formation in vibrated beds.[16]

Most studies of mixing or segregation behaviors of dry or wet granular materials in gas fluidized bed systems that have been reported in the literature to date have focused largely on the kinematics aspects of fluidization, mixing, and segregation behaviors. These do not provide deeper insights to the underlying mechanisms of the mixing or segregation behaviors that gave rise to such observations as low mixing efficiencies of wet granular materials in gas fluidized beds. To gain deeper insights to the fundamental mechanisms responsible for such fluidization, mixing, or segregation behaviors, considerations of the dynamics aspects are essential. In other words, analyses of the various forces present within the fluidized beds during fluidization, mixing, or segregation are required. These forces govern the fluid and particle behaviors which in turn determine the fluidization, mixing, and segregation behaviors of a fluidized bed. Quantitative comparisons of magnitudes of the various forces present during fluidization will potentially improve current understanding of the relative importance of these forces and how operating conditions can be controlled to enhance or diminish the effects of specific forces so as to either promote or inhibit mixing or segregation. Lim[17] applied a modified DEM incorporating additional force models for simulations of shear aggregation of colloidal nanoparticles and analyzed the time evolution of the various forces present to provide a more fundamental and mechanistic understanding of the shear aggregation process. In this study, the conventional CFD-DEM model was coupled with a capillary liquid bridge force model to investigate the mixing or segregation behaviors of dry and wet solid particles of different densities in gas fluidized beds. Mixing efficiencies were compared quantitatively via a mixing index and dynamic force data at the scale of individual particles were extracted from the simulations conducted and analyzed with a view toward advancing current understanding of the mechanisms involved in mixing or segregation of wet granular mixtures during fluidization processes. In the following section, the computational model and physical system of interest will be described. The simulation results obtained for the various physical conditions considered in this study will then be discussed and a summary of the conclusions derived will be presented in the Conclusions of this article.

Computational Model

Discrete element method

The DEM was developed by Cundall and Strack[18] for modeling the behavior of assemblies of discs and spheres. With the advent of computational power in recent years, it has been applied for studies of various types of multiphase systems.[19] In this section, a brief description of the method and corresponding governing equations will be presented.

The governing equations in DEM for describing translational and rotational motions of individual solid particles are basically Newton's laws of motion

$$m_i \frac{d\mathbf{v_i}}{dt} = \sum_{j=1}^{N} \left(\mathbf{f_{c,ij}} + \mathbf{f_{d,ij}}\right) + \mathbf{f_{f,i}} + \mathbf{f_{cap,ij}} + m_i \mathbf{g} \tag{1}$$

$$I_i \frac{d\boldsymbol{\omega}_\mathbf{i}}{dt} = \sum_{j=1}^{N} \mathbf{T_{ij}} \tag{2}$$

where m_i and $\mathbf{v_i}$ are the mass and velocity of the ith particle respectively, N is the number of particles in contact with the ith particle, $\mathbf{f_{c,ij}}$ and $\mathbf{f_{d,ij}}$ are the contact and viscous contact damping forces, respectively, $\mathbf{f_{f,i}}$ is the fluid drag force, $\mathbf{f_{cap,ij}}$ is the capillary liquid bridge force between wet particles, I_i is the moment of inertia of the ith particle, $\boldsymbol{\omega}_\mathbf{i}$ is its angular velocity and $\mathbf{T_{ij}}$ is the torque arising from contact forces which causes the particle to rotate. The torque $\mathbf{T_{ij}}$ is given by $\mathbf{T_{ij}} = \mathbf{f_{ct,ij}} \times \mathbf{R_i}$, where $\mathbf{f_{ct,ij}}$ is the tangential component of the contact force defined in the following force-displacement model.

Contact and damping forces were calculated by applying a linear spring-and-dashpot model as closure. The normal ($\mathbf{f_{cn,ij}}$, $\mathbf{f_{dn,ij}}$) and tangential ($\mathbf{f_{ct,ij}}$, $\mathbf{f_{dt,ij}}$) components of the contact and damping forces were calculated as follows

$$\mathbf{f_{cn,ij}} = -\left(\kappa_{n,i}\delta_{n,ij}\right)\mathbf{n_i} \tag{3}$$

$$\mathbf{f_{ct,ij}} = -\left(\kappa_{t,i}\delta_{t,ij}\right)\mathbf{t_i} \tag{4}$$

$$\mathbf{f_{dn,ij}} = -\eta_{n,i}(\mathbf{v_r} \cdot \mathbf{n_i})\mathbf{n_i} \tag{5}$$

$$\mathbf{f_{dt,ij}} = -\eta_{t,i}\left\{(\mathbf{v_r} \cdot \mathbf{t_i})\mathbf{t_i} + \left(\boldsymbol{\omega}_\mathbf{i} \times \mathbf{R_i} - \boldsymbol{\omega}_\mathbf{j} \times \mathbf{R_j}\right)\right\} \tag{6}$$

where $\kappa_{n,i}$, $\delta_{n,ij}$, $\mathbf{n_i}$, $\eta_{n,i}$, and $\kappa_{t,i}$, $\delta_{t,ij}$, $\mathbf{t_i}$, $\eta_{t,i}$ are the spring constants, displacements between particles, unit vectors and viscous contact damping coefficients in the normal and tangential directions, respectively, $\mathbf{v_r}$ is the relative velocity between particles and $\mathbf{R_i}$ and $\mathbf{R_j}$ are the radii of particles **i** and **j**, respectively. If $|\mathbf{f_{ct,ij}}| > |\mathbf{f_{cn,ij}}|\tan\phi$, then $|\mathbf{f_{ct,ij}}| = |\mathbf{f_{cn,ij}}|\tan\phi$, where $\tan\phi$ is analogous to the coefficient of friction.

Computational fluid dynamics

The governing equations for describing the motion of the continuum gas phase are basically the Navier-Stokes equations. An additional source term in the momentum equation has been included to account for interphase interactions

$$\frac{\partial \varepsilon}{\partial t}+\nabla \cdot (\varepsilon \mathbf{u})=0 \quad (7)$$

$$\frac{\partial (\rho_f \varepsilon \mathbf{u})}{\partial t}+\nabla \cdot (\rho_f \varepsilon \mathbf{u}\mathbf{u})=-\nabla P+\nabla \cdot (\mu_f \varepsilon \nabla \mathbf{u})+\rho_f \varepsilon \mathbf{g}-\mathbf{F} \quad (8)$$

where $\mathbf{u}$ is the velocity vector, ρ_f is the fluid density, μ_f is the fluid viscosity, ε is the local average porosity, P is the fluid pressure, and $\mathbf{F}$ is the source term due to fluid-particle interaction. The operating conditions imposed in this study were such that gas flows were nonturbulent and so a turbulence model was not applied in the solution of the gas flow field. It is well-established in the literature that two fundamental approaches, referred to as Model A and B, respectively, can be applied for treatments of fluid-particle interactions and pressure drop in a multiphase system. Feng and Yu[20] showed that significant differences existed in terms of solid flow patterns, mixing and segregation kinetics in numerical simulations of fluidization of binary mixtures of particles conducted using these two models. They concluded that simulation results obtained based on Model B compared more favorably with those of physical experiments. Following this study, the method of implementation of the CFD-DEM methodology as presented above followed that of Model B.

Fluid drag force

In a multiphase system, the interstitial fluid exerts drag forces on the solid particles whenever velocity differences exist between the two phases. Several fluid drag force models have been developed in the literature and the model due to Di Felice[21] which is applicable over a wide range of particle Reynolds numbers was used for calculating the fluid drag force in this study

$$\mathbf{f_{f,i}}=\mathbf{f_{f0,i}}\varepsilon_i^{-(\chi+1)} \quad (9)$$

$$\mathbf{f_{f0,i}}=0.5 c_{d0,i}\rho_f \pi R_i^2 \varepsilon_i^2 |\mathbf{u_i}-\mathbf{v_i}|(\mathbf{u_i}-\mathbf{v_i}) \quad (10)$$

$$\chi=3.7-0.65\exp\left[-\frac{\left(1.5-\log_{10} Re_{p,i}\right)^2}{2}\right] \quad (11)$$

$$c_{d0,i}=\left(0.63+\frac{4.8}{Re_{p,i}^{0.5}}\right)^2 \quad (12)$$

$$Re_{p,i}=\frac{2\rho_f R_i \varepsilon_i |\mathbf{u_i}-\mathbf{v_i}|}{\mu_f} \quad (13)$$

where $\mathbf{f_{f0,i}}$ is the fluid drag force on particle $\mathbf{i}$ in the absence of other particles, χ is an empirical parameter, ε_i is the local average porosity in the vicinity of particle i, $c_{d0,i}$ is the drag coefficient, $Re_{p,i}$ is the Reynolds number based on particle diameter and $\mathbf{u_i}$ is the fluid velocity of the computational cell in which particle i is located.

Capillary liquid bridge force

Several models for describing the behavior of liquid bridges between solid particles have been reported in the literature. In the current study, following Mikami et al.[11] and Lim et al.[13] the capillary liquid bridge force between wet particles was calculated according to the following equations

$$\hat{\mathbf{f}}_{\mathbf{cap,ij}}=\exp\left(A\hat{h}_c+B\right)+C \quad (14)$$

For particle-particle capillary liquid bridge force

$$\hat{h}_c=(0.62\theta+0.99)\hat{V}^{0.34} \quad (15)$$

$$A=-1.1\hat{V}^{-0.53} \quad (16)$$

$$B=\left(-0.34\ln\hat{V}-0.96\right)\theta^2-0.019\ln\hat{V}+0.48 \quad (17)$$

$$C=0.0042\ln\hat{V}+0.078 \quad (18)$$

For particle-wall capillary liquid bridge force

$$\hat{h}_c=(0.22\theta+0.95)\hat{V}^{0.32} \quad (19)$$

$$A=-1.9\hat{V}^{-0.51} \quad (20)$$

$$B=\left(-0.016\ln\hat{V}-0.76\right)\theta^2-0.12\ln\hat{V}+1.2 \quad (21)$$

$$C=0.013\ln\hat{V}+0.18 \quad (22)$$

where $\hat{h}_c=h_c/R_i$, $\hat{V}=V/\pi R_i^3$, $\hat{\mathbf{f}}_{\mathbf{cap,ij}}=\mathbf{f_{cap,ij}}/\pi R_i\gamma$, h_c is the critical rupture distance between particles, V is the liquid bridge volume, γ is the surface tension and, θ is the contact angle. In this capillary liquid bridge force model, the number of particle-particle and particle-wall contacts is not taken into consideration in calculating the capillary liquid bridge forces. The model also assumes that no transfer of liquid takes place between particles or between particles and wall so that the liquid bridge volume for each particle remains constant. Ennis et al.[22] showed that viscous effects dominated the capillary liquid bridge force when the capillary number, Ca, was greater than 1 and surface tension dominated it when Ca was less than 0.001. It was assumed that the viscous contribution to the strength of the capillary liquid bridge force was negligible for the physical conditions applied in this study. This assumption could be evaluated by examining the capillary number which is the ratio of the dynamic to static force, $Ca = \mu v_r/\gamma$, where μ is the liquid viscosity, v_r is the relative velocity between two particles connected by a liquid bridge and γ is the surface tension of the liquid. In this study, the liquid was assumed to be water and relative velocities between particles were not expected to be greater than 1 m s^{-1} for the operating conditions applied. Thus, the capillary number was expected to be less than about 0.01 which supports the assumption that the contribution of viscous effects to the capillary liquid bridge force could be deemed negligible compared to that of surface tension.

Simulation Conditions

The geometry of the computational domain considered in this study was a fluidized bed with a rectangular base measuring 15 cm × 6 cm and height of 120 cm. The granular materials consisted of a mixture of 36,000 particles with density 1400 kg m^{-3} (flotsam) and 20,000 particles with density 2600 kg m^{-3} (jetsam). Both flotsam and jetsam were spherical particles of diameter 3 mm. These material properties were based on the Eulerian-Lagrangian simulations carried out by Huilin et al.[10] A two-dimensional fluidized bed was considered by Huilin et al.[10] whereas a three-dimensional fluidized bed was simulated in the current study. In accordance with this scaling-up in the geometry, the amount of flotsam and jetsam particles was increased by 20 times in comparison with that used by Huilin et al.[10] while maintaining the mass fraction of flotsam to be 0.5 in accordance with the previous study so that qualitative comparisons between the simulation results could be made. Other pertinent material properties and simulation parameters are presented in Table 1. In all simulations performed, particles were first allowed to fall freely under

Table 1. Material Properties and System Parameters

Shape of Particles	Spherical
Number of flotsam particles	36,000
Number of jetsam particles	20,000
Particle diameter, d_p	3.0 mm
Density of flotsam particles	1400 kg m^{-3}
Density of jetsam particles	2600 kg m^{-3}
Coefficient of restitution	0.95, 0.99
Coefficient of friction	0.3
Gas density, ρ_f	1.205 kg m^{-3}
Gas viscosity, μ_f	1.8×10^{-5} N s m^{-2}
Gas velocity	1.8, 2.3, 2.8 m s^{-1}
Amount of liquid present	0.0, 0.05, 0.1, 0.5, 0.8, 1.0 wt %
Surface tension, γ	0.073 N m^{-1}
Contact angle, θ	0 rad
System dimensions	15 cm length × 6 cm width × 120 cm height
Simulation time step, Δt	10^{-6} s

gravity for 0.5 s to form a bed at the bottom of the container before fluidizing air was introduced. A uniform fluidizing gas velocity was applied at the base of the computational domain to simulate a uniform gas distribution. Simulations for both solid and gas phases were performed in three dimensions.

The packed bed formed at the start of each fluidization process was divided into three zones and the flotsam and jetsam particles in the three zones were colored differently to allow visualization of the subsequent mixing or segregation behaviors. The first zone at the bottom of the bed consisted of 10,000 flotsam particles marked in blue. The second zone in the middle of the bed was a well-mixed region containing 20,000 flotsam particles marked in orange and 20,000 jetsam particles marked in yellow. The flotsam and jetsam particles were placed in alternating positions within this zone to simulate a state of perfect mixing as the initial condition for this zone. The third zone at the top of the bed consisted of 6000 flotsam particles marked in red. These three zones will be referred to as Zones 1 (bottom), 2 (middle), and 3 (top), respectively. Such an initial configuration of the fluidized bed comprising both segregated and well-mixed regions was considered to impose less bias on the subsequent mixing or segregation behavior of the bed, as it would not be known before simulation whether the mixture would have a tendency to mix or segregate.

Results and Discussion

Dry particle fluidization

The CFD-DEM model was first used for numerical simulations of dry granular materials with different densities. Figure 1 shows the mixing or segregation behaviors of the particles during fluidization at three different fluidizing velocities when the coefficient of restitution was $e = 0.95$. With a fluidizing velocity of 1.8 m s^{-1}, Figure 1a shows that the bed of particles had become fairly segregated at the end of 5 s. Flotsam particles near the bottom of the bed (blue) were lifted upward within 1.5 s of the start of fluidization. As fluidization continued, more orange flotsam particles started to migrate toward the top of the bed to mix with the blue and red flotsam particles. The final state of the bed consisted of a fluidized layer of flotsam particles and a defluidized layer of jetsam particles. When the fluidizing velocity was increased to 2.3 m s^{-1}, Figure 1b shows that particles were able to undergo more vigorous fluidization. In contrast to the previous case, blue and orange flotsam particles migrated toward the top of the bed to form a relatively well-mixed region within 3.0 s of the start of fluidization. As fluidization continued, jetsam particles were able to mix with the flotsam particles, resulting in only a portion of them settling at the bottom of the bed. With an even higher fluidizing velocity of 2.8 m s^{-1}, Figure 1c shows that the bed expanded to larger extents as compared with the previous cases. A large portion of jetsam particles still remained at the bottom of the bed after 3.0 s. However, through further fluidization, a relatively well-mixed bed was eventually formed.

Figure 2 shows the mixing or segregation behaviors of the particles during fluidization at three different fluidizing velocities when $e = 0.99$. With a fluidizing velocity of 1.8 m s^{-1}, Figure 2a shows that mixing and segregation behaviors were similar to those where $e = 0.95$. However, when fluidizing velocity was increased to 2.3 m s^{-1}, Figure 2b shows that a large portion of jetsam particles migrated to the top of the bed to form a relatively well-mixed bed with the flotsam particles within 3.0 s after the gas was introduced, and no apparent segregation was observed by the end of the simulation. With an even higher fluidizing velocity of 2.8 m s^{-1}, Figure 2c shows that the bed profile approached a well-mixed state and appeared to have reached a steady state at about 3.0 s. These observations suggested that an increase in coefficient of restitution improved mixing behaviors, especially at a higher fluidizing velocity. This was likely due to reduced dissipation of kinetic energy during particle-particle collisions when $e = 0.99$.

Figure 3 compares mass fraction distributions of flotsam particles computed via Eulerian-Lagrangian simulations by Huilin et al.[10] with those computed via CFD-DEM simulations in the present study for different coefficients of restitution and fluidizing velocities. These comparisons were conducted to show consistency in the behaviors of the fluidized bed observed in the simulations in the sense that segregation between the flotsam and jetsam particles were observed in both the current simulations and those reported by Huilin et al.[10] In all cases, the mass fractions of flotsam particles were higher near the top of the bed and lower near the bottom, indicating the presence of segregation behaviors within the bed. The degree of segregation decreased and mixing improved when fluidizing velocity and coefficient of restitution increased. Good qualitative agreement between the current CFD-DEM simulation results and the Eulerian-Lagrangian simulation results reported by Huilin et al.[10] was achieved. The discrepancies observed between the two sets of results might be attributed to the fact that the fluidized bed simulated using the Eulerian-Lagrangian approach by Huilin et al.[10] was two-dimensional while the one simulated using the CFD-DEM approach in the present study was three-dimensional, and considered mixing behaviors in all three directions.

Figures 4 and 5 show the distributions of flotsam and jetsam particles originally belonging to various zones within the fluidized bed for the different fluidizing velocities applied for $e = 0.95$ and $e = 0.99$, respectively. Although bed heights were generally larger with higher fluidizing velocities, the number of particles near the top of the bed might be low such as to give rise to large fluctuations in the number fraction distribution profiles. As such, profiles for a representative section of each fluidized bed rather than the entire bed height was plotted to allow the state of segregation to be discerned. The vertical, dotted lines (from left to right) represent the number fraction of flotsam in Zone 3, flotsam in Zone 1, and flotsam

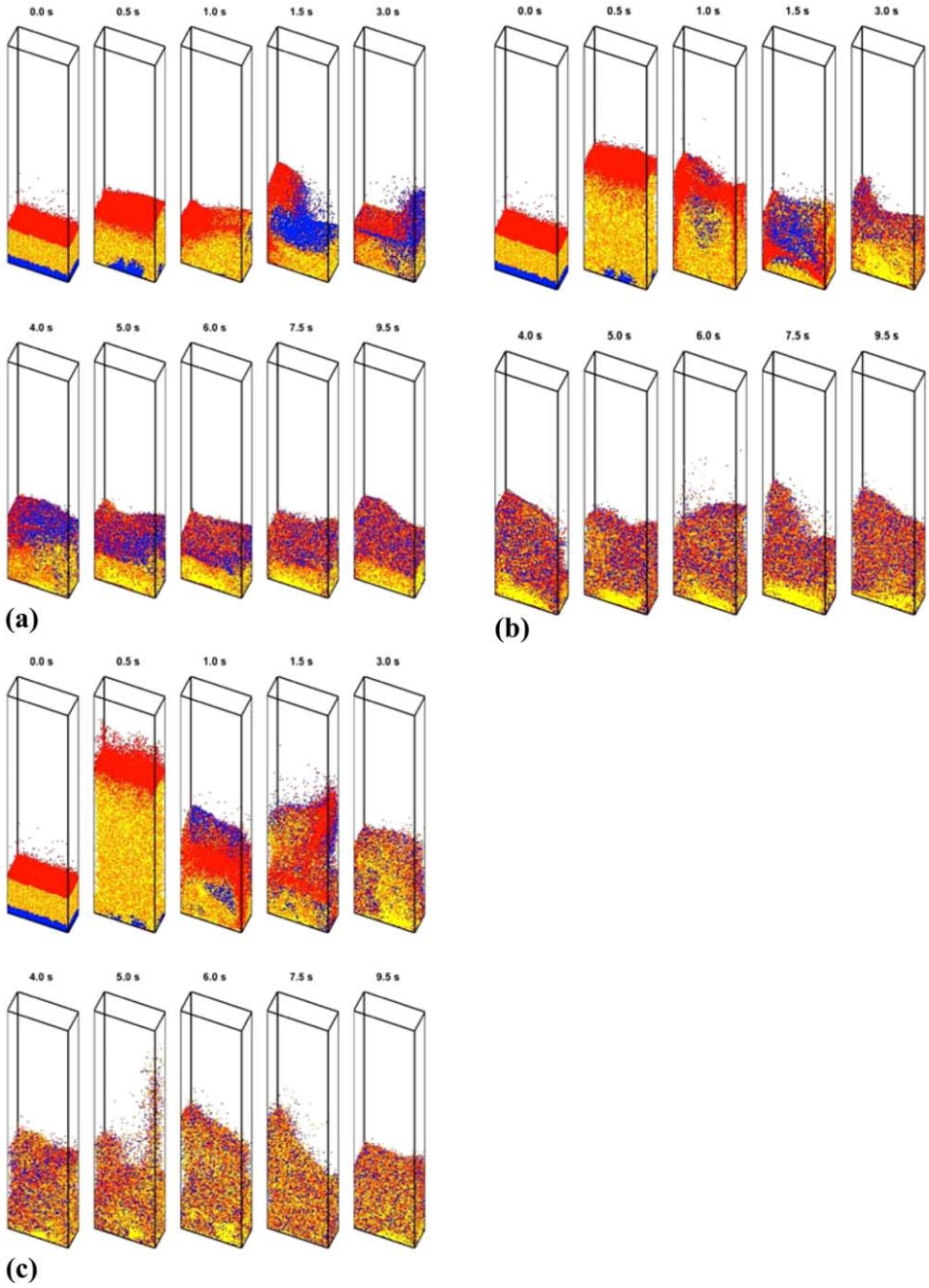

Figure 1. Mixing behaviors of dry particles with different densities ($e = 0.95$) for fluidizing velocities of (a) 1.8 m s^{-1}, (b) 2.3 m s^{-1} and (c) 2.8 m s^{-1}.

and jetsam in Zone 2 in the entire system, respectively for a perfectly well-mixed bed. With increasing fluidizing velocities, it may be observed that the amount of jetsam particles near the bottom of the bed decreased and the particles became more uniformly distributed over the height of the bed at both coefficients of restitution. This indicated a smaller density segregation effect at higher fluidizing velocity. For the same fluidizing velocity, more jetsam particles were found at the bottom of the bed for $e = 0.95$ as compared to $e = 0.99$, which again indicated better mixing at higher coefficient of restitution.

The progressions in time of the extents of mixing or segregation may also be analyzed based on a mixing index.[23–25] Here, the Lacey mixing index was calculated at equal time intervals of 0.01 s during the fluidization process for each fluidized bed according to the following formula

$$\text{Lacey index} = \frac{\sigma_o^2 - \sigma^2}{\sigma_o^2 - \sigma_R^2} \tag{23}$$

where σ_o^2 and σ_R^2 are the theoretical upper and lower limits of mixture variances calculated as $\sigma_o^2 = p\ (1-p)$ and $\sigma_R^2 = p\ (1-p)/n$, p and $(1-p)$ are the proportions of flotsam and jetsam particles respectively determined from samples and n is the number of particles in each sample. A Lacey index of 1 represents a perfectly well-mixed bed whereas a Lacey index

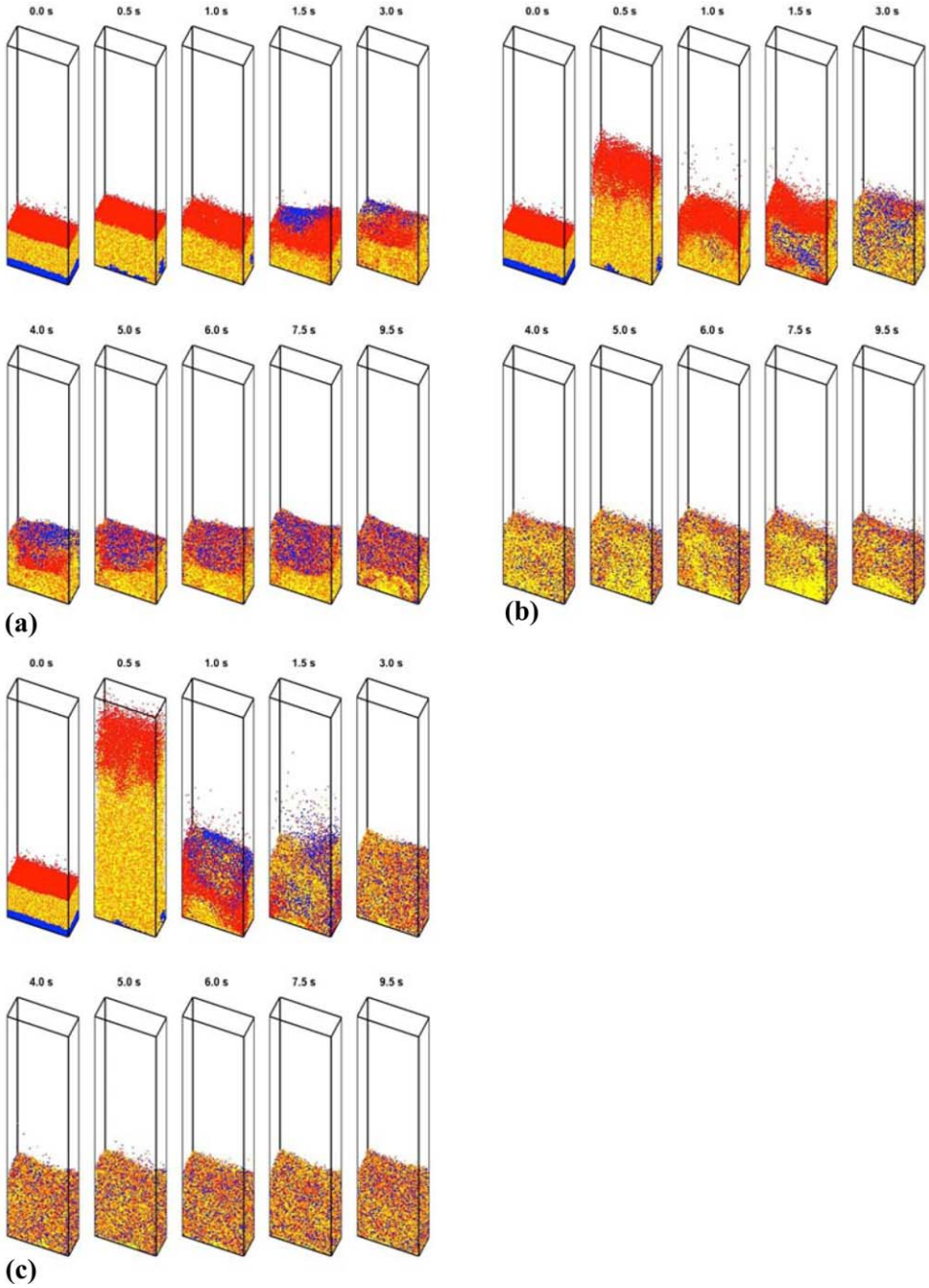

Figure 2. Mixing behaviors of dry particles with different densities ($e = 0.99$) for fluidizing velocities of (a) 1.8 m s^{-1}, (b) 2.3 m s^{-1} and (c) 2.8 m s^{-1}.

[Color figure can be viewed in the online issue, which is available at wileyonlinelibrary.com.]

of 0 represents a perfectly segregated bed. The computational domain was divided into sampling cells with dimensions 10 mm × 10 mm × 10 mm for sampling. Sampling was performed on every cell at equal time intervals and only samples containing at least 30 particles were used for calculating the Lacey mixing index. At the start of the fluidization process, the Lacey mixing index value for each fluidized bed system was about 0.85, indicating an overall well-mixed state. This was due to the state of perfect mixing imposed as an initial condition for Zone 2 which would then have a local Lacey mixing index value of 1.0.

Figures 6a and b show the time evolution of Lacey index values for fluidized beds containing dry granular mixtures at different fluidizing velocities for $e = 0.95$ and $e = 0.99$ respectively. Feng et al.[23] previously showed that the Lacey mixing index values of fluidized beds undergoing mixing or segregation would reach a dynamically stable value when a dynamic equilibrium state was attained. Here, the Lacey index values did not reach dynamically stable values for some of the fluidized bed systems considered indicating that a dynamically stable state was not attained yet within 10 s of fluidization. Nevertheless, the time evolution of mixing index values in the first 10 s can be a good indication of the tendency for a particular fluidized bed system to undergo mixing or segregation and how efficient the process is likely to be. It may be observed that a higher coefficient of restitution led to better

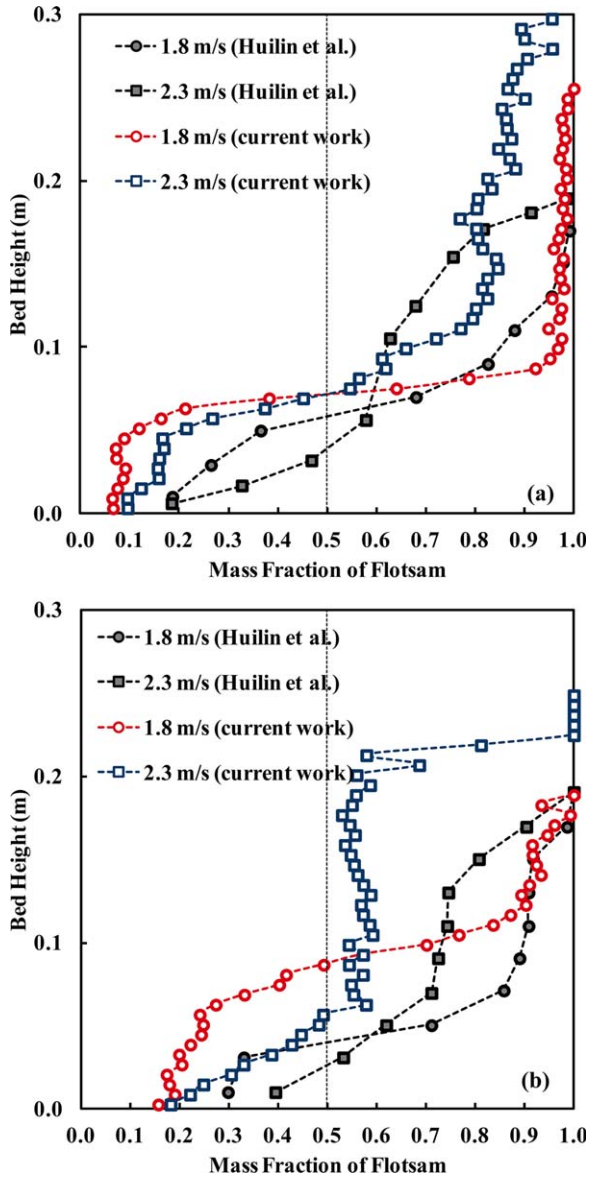

Figure 3. Comparisons of mass fraction distributions of flotsam particles between Eulerian-Lagrangian simulation results of Huilin et al.[10] and current CFD-DEM simulation results for (a) $e = 0.95$ and (b) $e = 0.99$.

The fluidizing velocities applied were 1.8 m s^{-1} and 2.3 m s^{-1}. [Color figure can be viewed in the online issue, which is available at wileyonlinelibrary.com.]

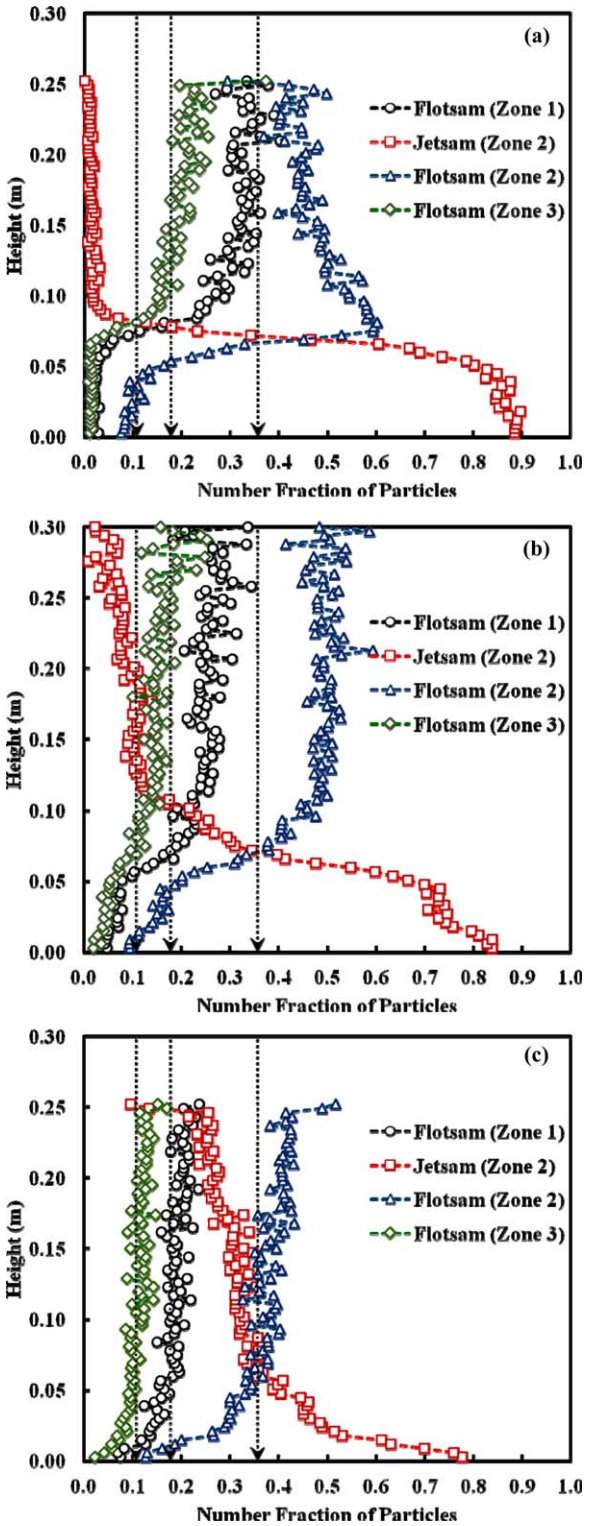

Figure 4. Distributions of dry particles originally belonging to various zones within the fluidized bed for $e = 0.95$ at the end of 10 s.

The fluidizing velocities applied were (a) 1.8 m s^{-1}, (b) 2.3 m s^{-1} and (c) 2.8 m s^{-1}. [Color figure can be viewed in the online issue, which is available at wileyonlinelibrary.com.]

mixing efficiencies. For a coefficient of restitution of 0.95, the Lacey index values decreased fairly rapidly for fluidizing velocities of 1.8 m s^{-1} and 2.3 m s^{-1}, indicating density segregation of particles, while the values remained fairly high throughout the fluidization process for a fluidizing velocity of 2.8 m s^{-1}. For a coefficient of restitution of 0.99, the Lacey index value decreased less rapidly as compared to when $e = 0.95$ for a fluidizing velocity of 1.8 m s^{-1}. Nevertheless, the decreasing trend was still indicative of segregation occurring within the system. The Lacey mixing indices for fluidizing velocities of 2.3 m s^{-1} and 2.8 m s^{-1}, on the other hand, remained fairly constant at about 0.80 after a simulation time of 3.0 s, which suggested that both beds remained fairly well-mixed throughout the fluidization process. These observations were in agreement with those derived based on visual inspections of Figures 1 and 2 previously.

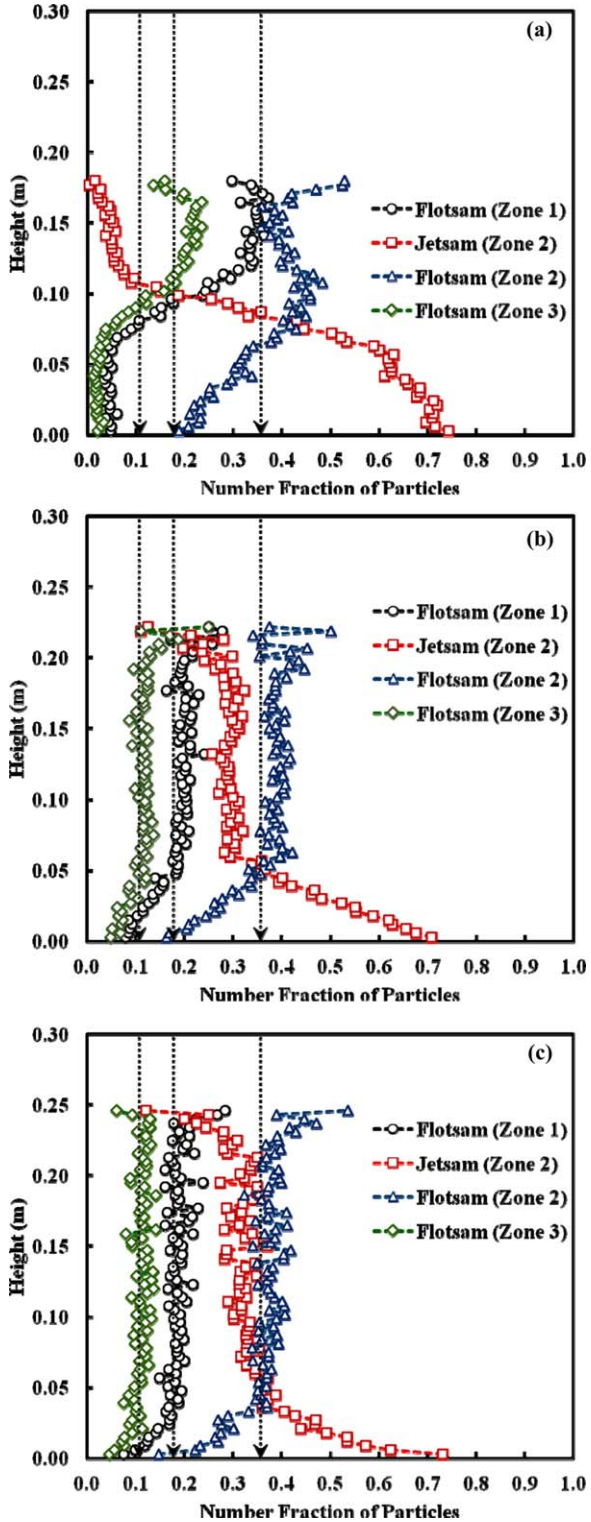

Figure 5. Distributions of dry particles originally belonging to various zones within the fluidized bed for $e = 0.99$ at the end of 10 s.

The fluidizing velocities applied were (a) 1.8 m s^{-1}, (b) 2.3 m s^{-1} and (c) 2.8 m s^{-1}. [Color figure can be viewed in the online issue, which is available at wileyonlinelibrary.com.]

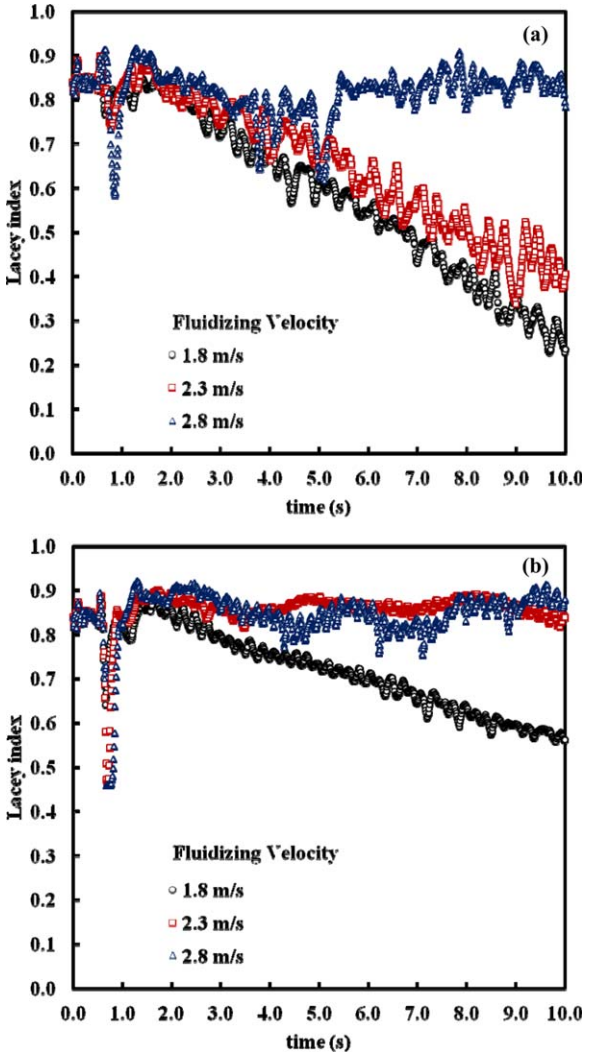

Figure 6. Time evolution of Lacey mixing indices for the fluidized bed systems containing dry particles at different fluidizing velocities for (a) $e = 0.95$ and (b) $e = 0.99$.

[Color figure can be viewed in the online issue, which is available at wileyonlinelibrary.com.]

Figure 7 shows snapshots of velocity vectors of dry particles ($e = 0.95$) at fluidizing velocities of 1.8 m s^{-1} and 2.8 m s^{-1}. A region of only one particle diameter in thickness extracted from the midplane of the bed along the spanwise direction is presented to allow better visualization of particle movements within the bed. At the fluidizing velocity of 2.8 m s^{-1}, magnitudes of particle velocities were observed to be sufficiently high to allow some jetsam particles to move to the top of the bed. However, some jetsam particles were observed to move near the bottom of the bed with low velocities. This segregation between flotsam and jetsam particles resulted in the Lacey index values not increasing towards 1.0 even when a fluidizing velocity of 2.8 m s^{-1} was applied.

Figure 8 shows the time evolution of average relative fluid drag forces ($\mathbf{f}_{drag}/\mathbf{f}_g$) for flotsam and jetsam particles originally belonging to various zones within the fluidized bed for $e = 0.95$ at different fluidizing velocities. These were calculated by averaging over all particles in the entire bed and nondimensionalizing by the particle weight of each zone, $\mathbf{f}_g$, at every time step. With a fluidizing velocity of 1.8 m s^{-1}, drag forces acting on the flotsam particles in Zones 1 (bottom) and 2 (middle) were larger than those acting on flotsam particles in

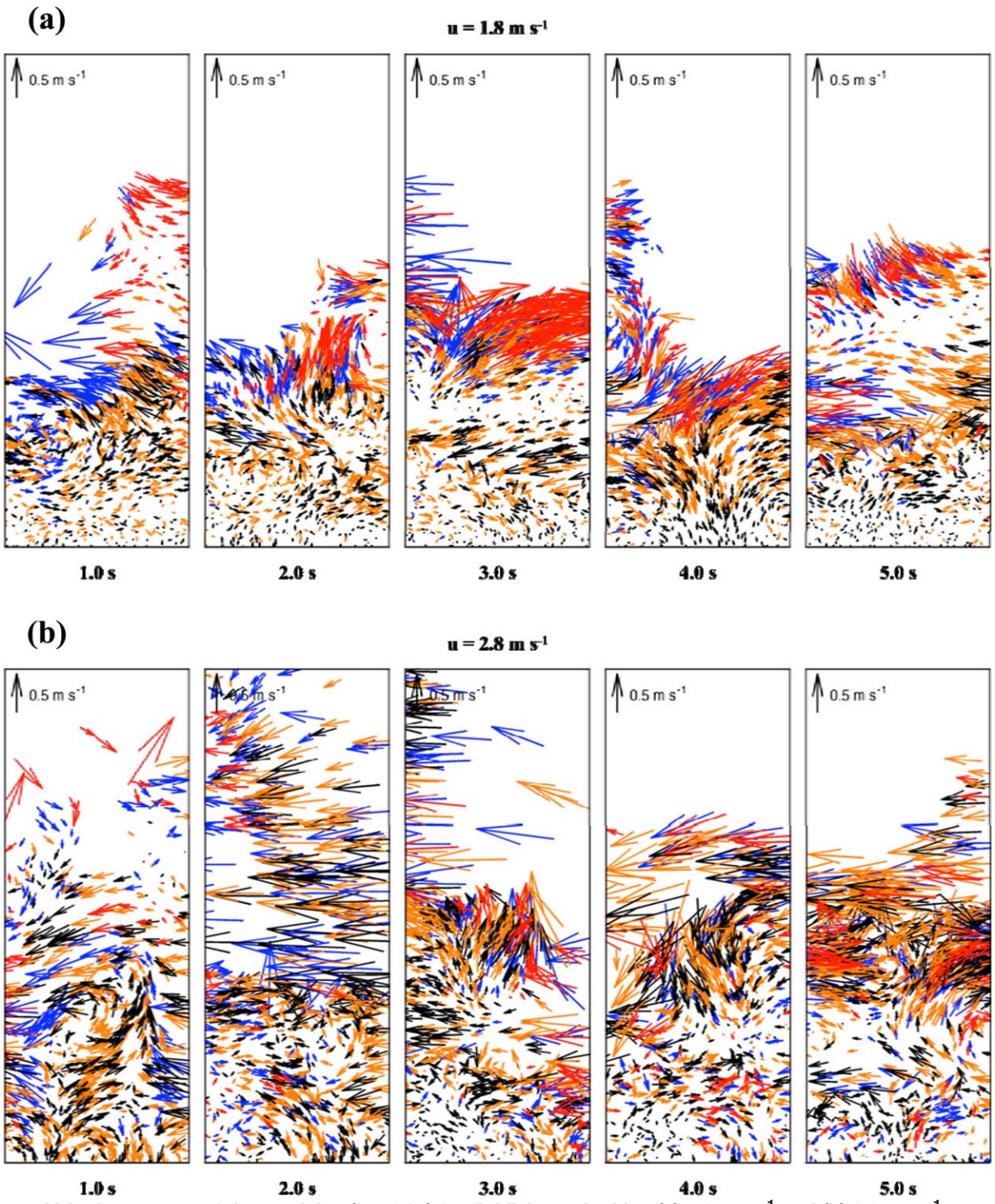

Figure 7. Velocity vectors of dry particles ($e = 0.95$) for fluidizing velocities (a) 1.8 m s^{-1} and (b) 2.8 m s^{-1}.

[Color figure can be viewed in the online issue, which is available at wileyonlinelibrary.com.]

Zone 3 (top) for the first 1.5 s of fluidization, suggesting that there would be an initial net upward movement of these particles towards the top of the bed. As fluidization continued, drag forces acting on the flotsam particles in Zones 1 and 3 fluctuated around $\mathbf{f_{drag}}/\mathbf{f_g} = 1$ whereas drag forces acting on the flotsam particles in Zone 2 were larger than those in Zones 1 and 3. As the flotsam particles in Zone 2 were initially positioned between jetsam particles, the larger drag forces might have contributed towards moving these flotsam particles through the well-mixed region. This also indicated that there was a net upward movement of flotsam particles in Zone 2 towards the top of the bed during the fluidization process.

These observations were consistent with the density segregation behaviors observed in Figure 1a earlier, with most of the blue flotsam particles being carried to the top of the bed shortly after the fluidizing gas was introduced while orange flotsam particles continued to migrate toward the top flotsam layer as fluidization proceeded. It may also be observed that

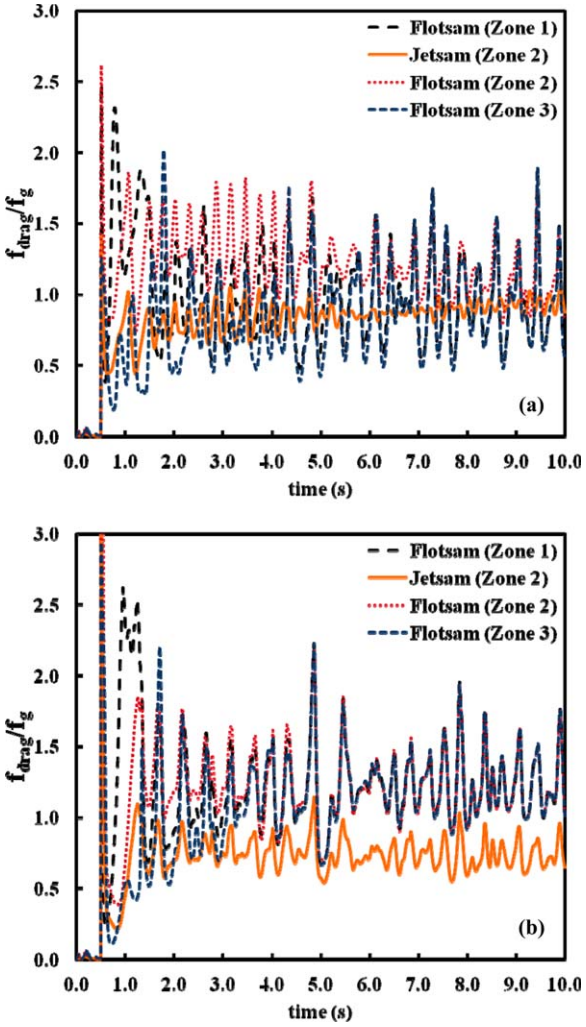

Figure 8. Time evolution of average relative fluid drag forces (f_{drag}/f_g) for dry particles ($e = 0.95$) originally belonging to various zones within the fluidized bed.

The fluidizing velocities applied were (a) 1.8 m s^{-1} and (b) 2.8 m s^{-1}. [Color figure can be viewed in the online issue, which is available at wileyonlinelibrary.com.]

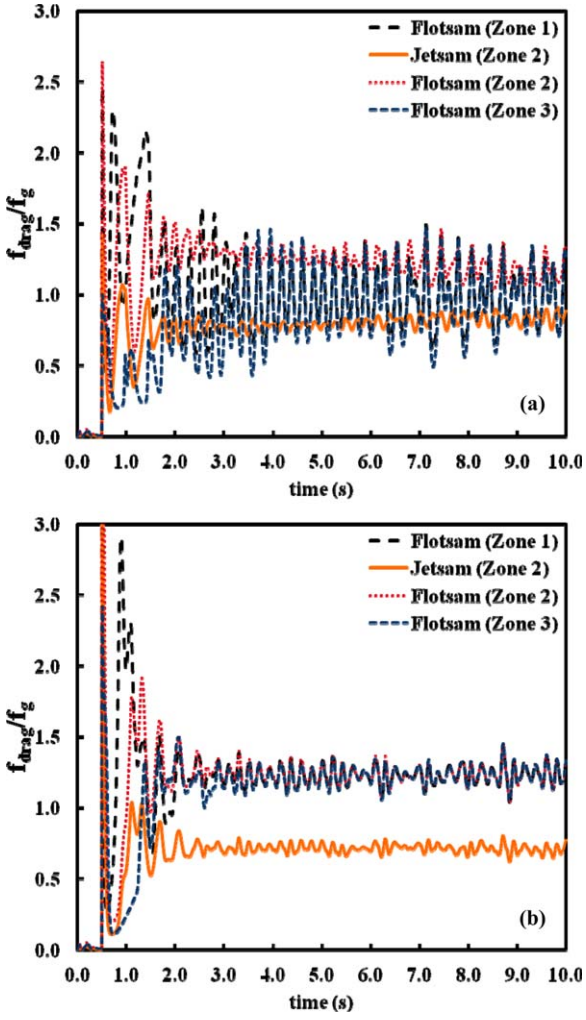

Figure 9. Time evolution of average relative fluid drag forces (f_{drag}/f_g) for dry particles ($e = 0.99$) originally belonging to various zones within the fluidized bed.

The fluidizing velocities applied were (a) 1.8 m s^{-1} and (b) 2.8 m s^{-1}. [Color figure can be viewed in the online issue, which is available at wileyonlinelibrary.com.]

after approximately 3.5 s of fluidization, the average drag forces acting on flotsam particles in Zones 1 and 3 converged, indicating that the behaviors of particles had become independent of the initial state of the bed. However, the time taken for the average drag forces acting on flotsam particles in Zone 2 to converge with those in the other two zones was much longer. This might be due to a lower efficiency in separating out flotsam particles from a well-mixed zone to form a segregated state with flotsam particles near the top of the bed compared with forming a segregated state from an initial state where flotsam particles occupied the bottom region of the bed. In the latter case, drag forces acting on flotsam particles in Zone 1 shortly after the fluidizing gas was introduced would be large enough for these flotsam particles to be lifted through Zones 2 and 3. With a fluidizing velocity of 2.8 m s^{-1}, the time taken for average drag forces acting on flotsam particles in all zones to converge was much shorter. This might be due to larger drag forces acting on the particles at the higher fluidizing velocity, allowing the particles to form a well-mixed bed as observed previously, and consequently becoming independent of the initial state more quickly.

Figure 9 shows the time evolution of average relative fluid drag forces ($\mathbf{f}_{drag}/\mathbf{f}_g$) for $e = 0.99$ at different fluidizing velocities. Fluctuations in drag forces decreased at a higher coefficient of restitution, which was consistent with previous observations. Similar to the CFD-DEM simulations by Feng et al.[23] two stages could be observed: a transient stage and a pseudosteady stage. In the transient stage, drag forces acting on both flotsam and jetsam particles increased with time, which corresponded with mixing or segregation of the bed. In the pseudosteady stage, however, the forces fluctuated about a mean value, indicating that a macroscopically pseudosteady state had been attained. This was more apparent in Figure 9 due to less vigorous fluctuations of the drag forces. The time to reach the pseudosteady stage was approximately 7 s and 2 s for a fluidizing velocity of 1.8 m s^{-1} and 2.8 m s^{-1}, respectively.

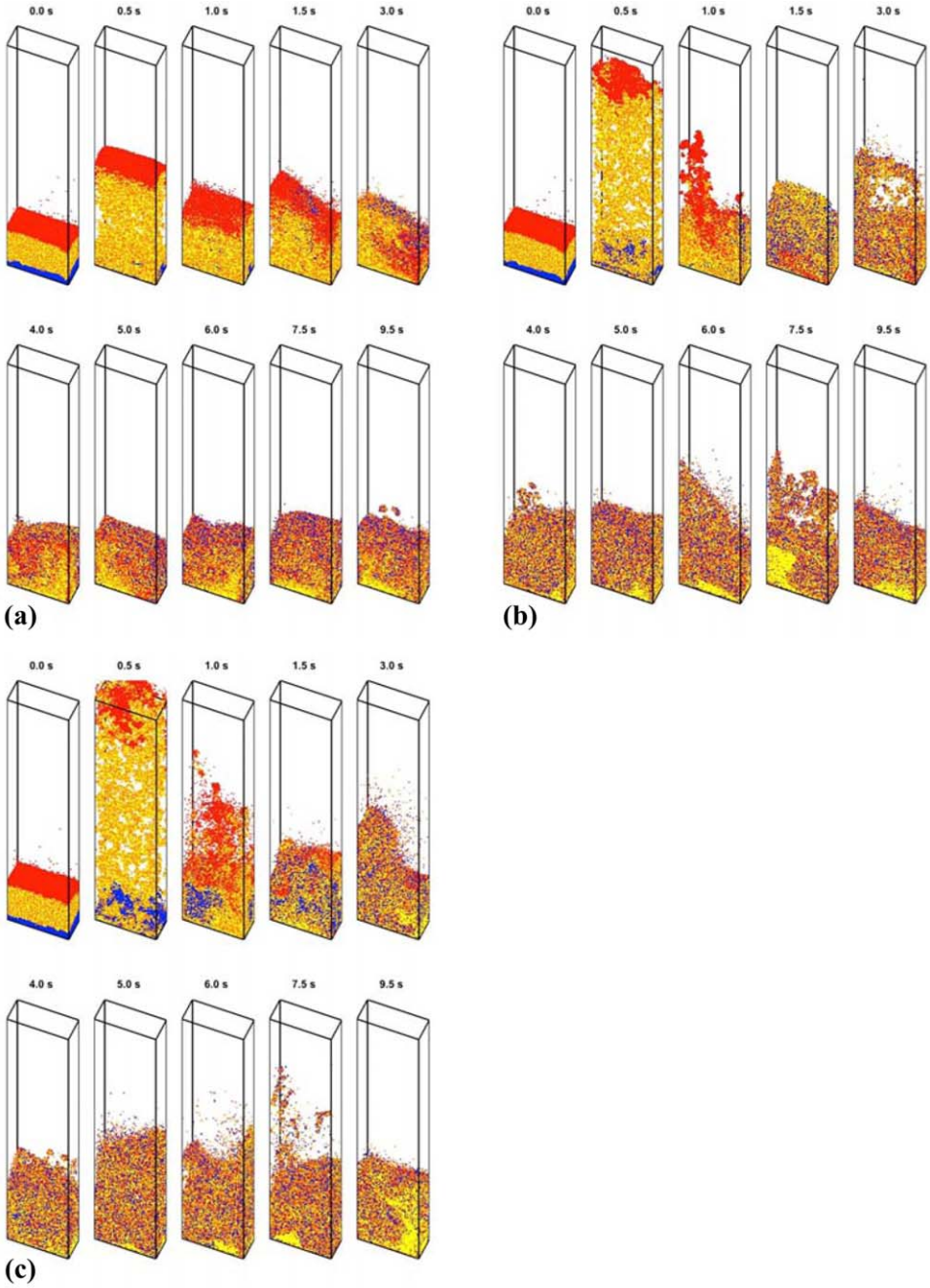

Figure 10. Mixing behaviors of wet particles with different densities ($e = 0.95$) for fluidizing velocities of (a) 1.8 m s^{-1}, (b) 2.3 m s^{-1} and (c) 2.8 m s^{-1}.

The amount of liquid present was simulated to be 0.1 wt %.

Wet particle fluidization

Figures 10 and 11 show the mixing behaviors of wet particles ($e = 0.95$) at different fluidizing gas velocities with small amounts of liquid equivalent to 0.1 wt % and 1.0 wt % of the total weight of particles respectively. Unlike the fluidization behaviors observed previously in Figures 1a and b, density segregation at 1.8 m s^{-1} and 2.3 m s^{-1} was significantly suppressed even in the presence of only 0.1 wt % liquid. The predominant behavior of the bed appeared to be gradual mixing between the flotsam and jetsam particles for the fluidizing velocities considered. Particles also exhibited higher tendencies to form agglomerates and fluidization was more sluggish as the amount of liquid increased. The final states of the mixtures after a simulation time of 10 s were more well-mixed with increasing fluidizing velocity.

Figure 12 shows the mass fraction distributions of flotsam particles for different fluidizing velocities applied. The amounts of liquid present were simulated to be 0.1 wt % and 1.0 wt %. It may be observed that the particles approached a well-mixed state when the amount of liquid present increased, indicating a decrease in tendency for density segregation. For beds containing 1.0 wt % liquid at fluidizing velocities of 2.3 m s^{-1} and 2.8 m s^{-1}, the distribution profiles collapsed onto the dotted

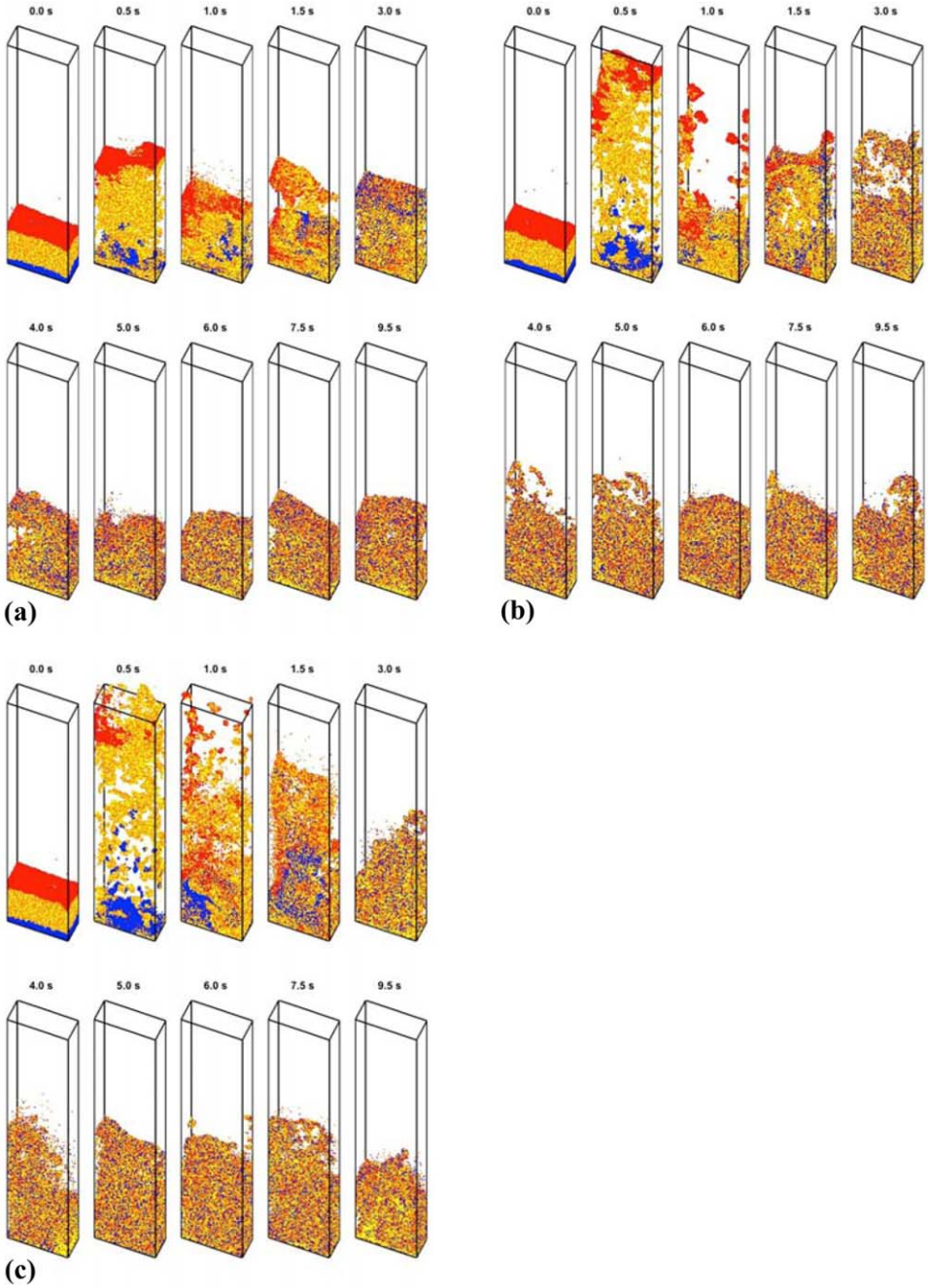

Figure 11. Mixing behaviors of wet particles with different densities ($e = 0.95$) for fluidizing velocities of (a) 1.8 m s^{-1}, (b) 2.3 m s^{-1} and (c) 2.8 m s^{-1}.

The amount of liquid present was simulated to be 1.0 wt %. [Color figure can be viewed in the online issue, which is available at wileyonlinelibrary.com.]

lines over most parts of the beds, suggesting that the beds had reached well-mixed states after 10 s of fluidization. In general, beds containing wet granular mixtures evolved into more well-mixed states than those containing dry granular mixtures.

Figure 13 shows the time evolution of Lacey index values for fluidized beds containing dry or wet granular mixtures with different fluidizing velocities applied. At the start of the fluidization process, a small increase in Lacey index values for all fluidized beds was observed. This might be due to the initial large expansion of the beds from a compact, packed bed state which resulted in a small extent of mixing between the flotsam and jetsam particles. With a fluidizing velocity of 1.8 m s^{-1}, the Lacey index values dropped much more rapidly for dry particles as compared to wet particles containing 0.1 wt % liquid, while they remained fairly high throughout the fluidization process for the bed containing 1.0 wt % liquid, indicating a lower rate of density segregation for wet particles. This might be a result of wet particles forming agglomerates with neighboring particles prior to fluidization, making it harder to separate flotsam particles from jetsam particles, and hence hindering mixing or segregation. When the fluidizing velocity was increased to 2.3 m s^{-1}, mixing efficiencies of particles with the different amounts of liquid simulated improved, which was consistent with the corresponding

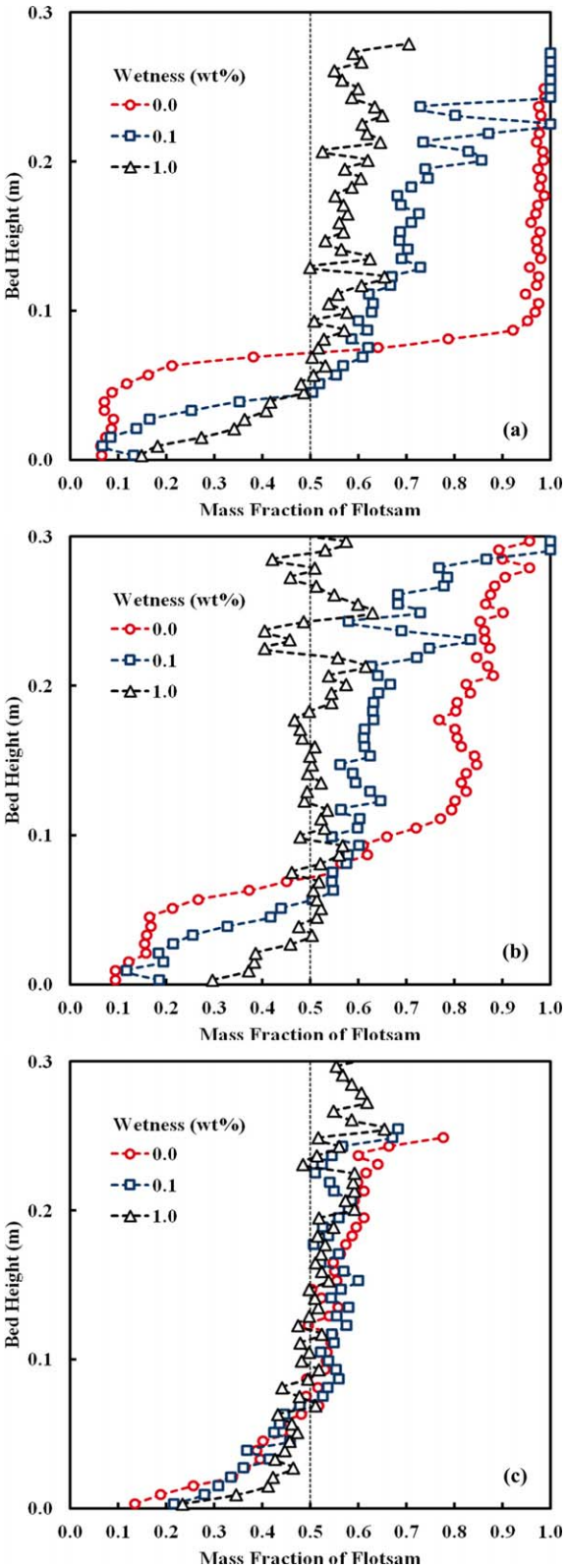

Figure 12. Mass fraction distributions of flotsam particles with different amounts of liquid at the end of 10 s.

The fluidizing velocities applied were (a) 1.8 m s^{-1}, (b) 2.3 m s^{-1} and (c) 2.8 m s^{-1}. [Color figure can be viewed in the online issue, which is available at wileyonlinelibrary.com.]

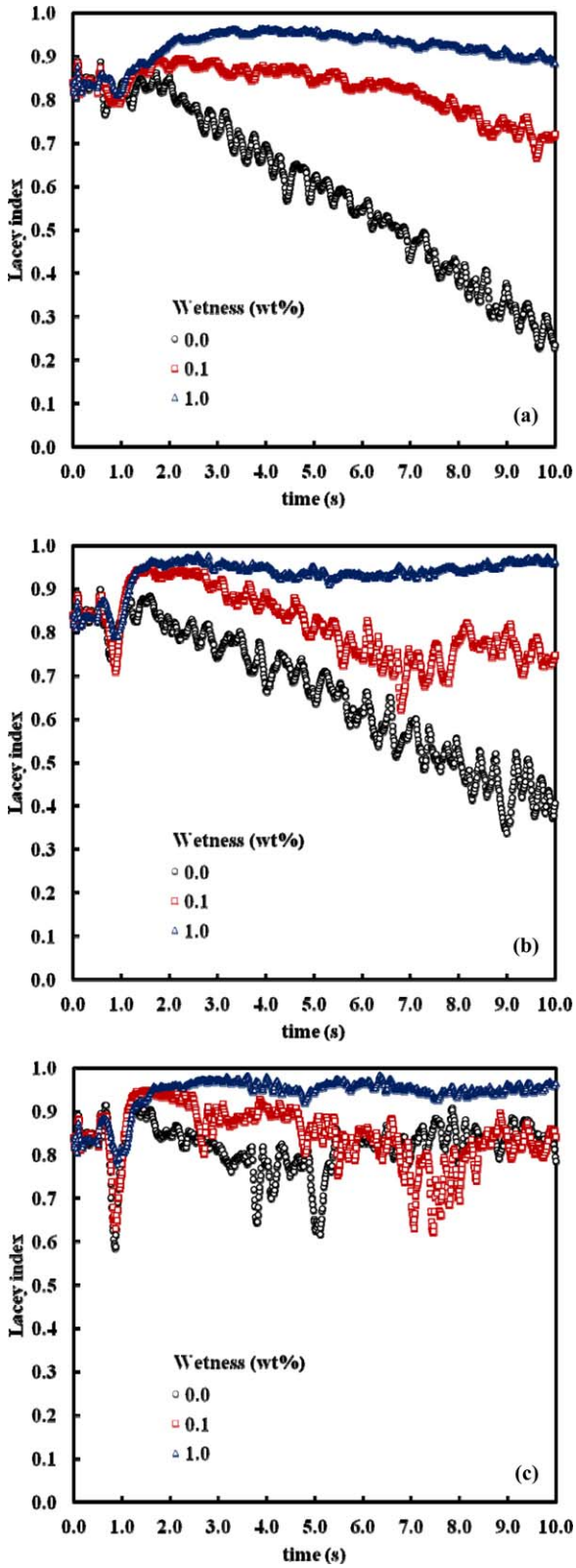

Figure 13. Time evolution of Lacey mixing indices for fluidized beds containing dry particles or wet particles with 0.1 wt % or 1.0 wt % liquid.

The fluidizing velocities applied were (a) 1.8 m s^{-1}, (b) 2.3 m s^{-1} and (c) 2.8 m s^{-1}. [Color figure can be viewed in the online issue, which is available at wileyonlinelibrary.com.]

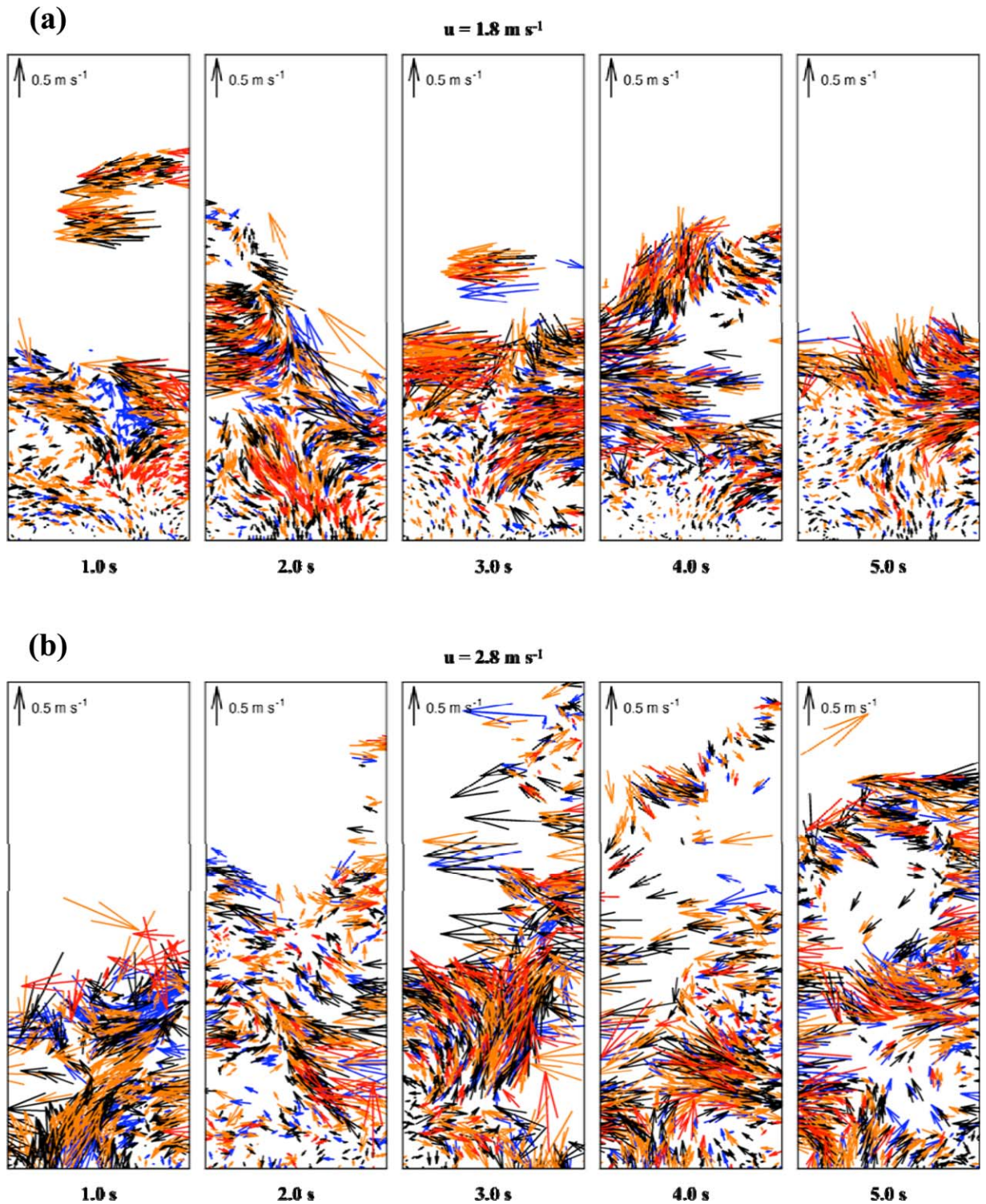

Figure 14. Velocity vectors of wet particles ($e = 0.95$) for fluidizing velocities (a) 1.8 m s^{-1} and (b) 2.8 m s^{-1}.

The amount of liquid present was simulated to be 1.0 wt %. [Color figure can be viewed in the online issue, which is available at wileyonlinelibrary.com.]

mixing behaviors of dry particles. When the amount of liquid present was 1.0 wt %, the Lacey index values remained fairly constant at about 0.95 shortly after the fluidizing gas was introduced whereas the values decreased for 0.1 wt % liquid. This again suggested that the tendency for density segregation was reduced in the presence of a larger amount of liquid in bed. With an even higher fluidizing velocity of 2.8 m s^{-1}, the Lacey indices remained fairly high throughout the fluidization process for the beds containing dry and wet particles. These trends were indicative of the beds becoming well-mixed and were in agreement with those derived based on visual inspections of Figures 10 and 11. In addition, since the mixing indices did not increase much when the fluidizing velocity was increased from 2.3 m s^{-1} to 2.8 m s^{-1} for beds containing 1.0 wt % liquid, it suggested that the mixtures remained fairly well-mixed throughout the fluidization process. It appeared

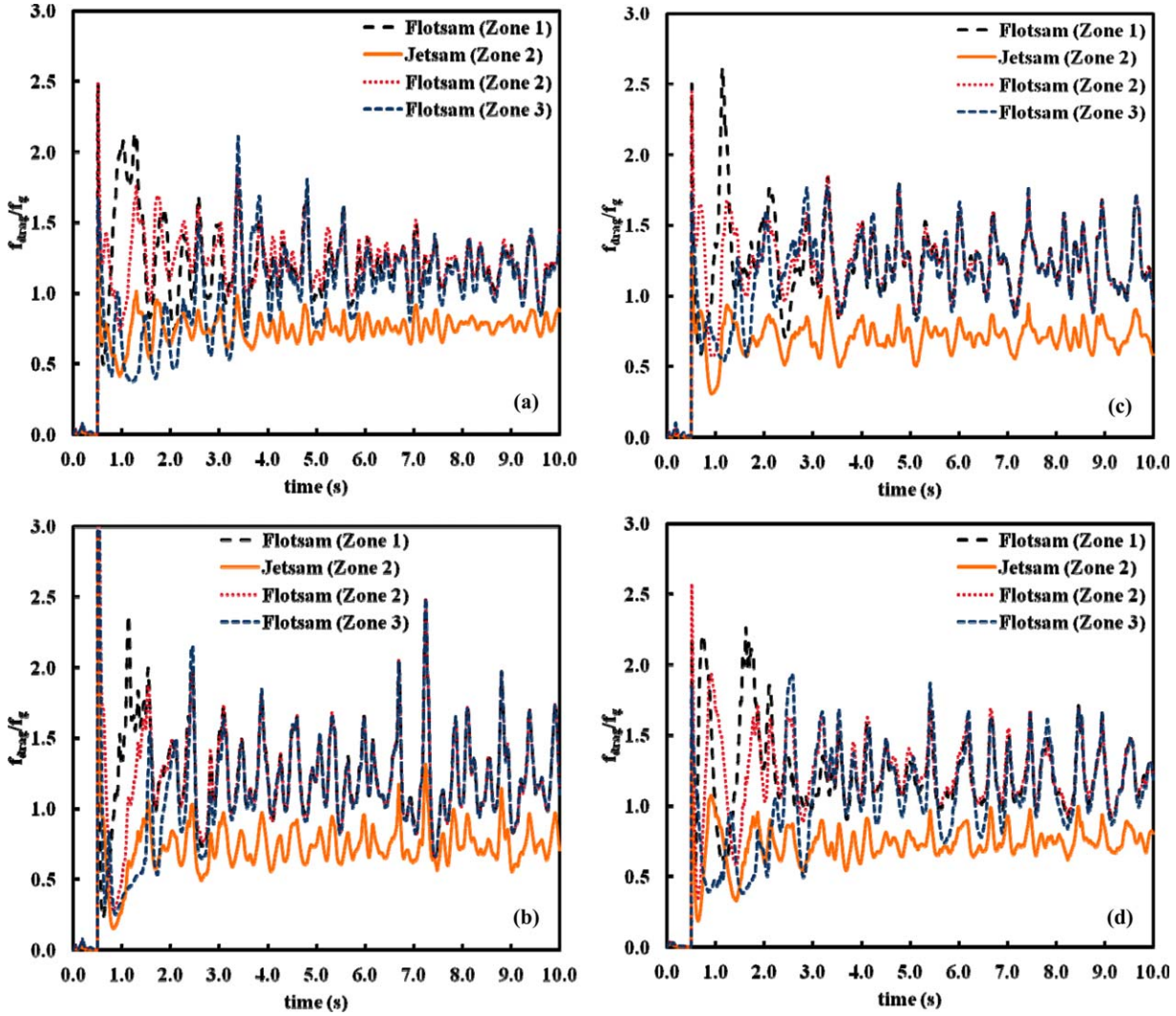

Figure 15. Time evolution of average relative fluid drag forces (f_{drag}/f_g) for wet particles ($e = 0.95$) originally belonging to various zones within the fluidized bed.

The amounts of liquid present and fluidizing velocities applied were (a) 0.1 wt % and 1.8 m s^{-1}, (b) 0.1 wt % and 2.8 m s^{-1}, (c) 1.0 wt % and 1.8 m s^{-1}, and (d) 1.0 wt % and 2.8 m s^{-1}. [Color figure can be viewed in the online issue, which is available at wileyonlinelibrary.com.]

then that there were two mechanisms that contributed to the high Lacey index values: more vigorous motions of particles resulting from higher fluidizing velocities as well as stronger capillary liquid bridge forces which hindered relative motions between particles and hence suppressed density segregation.

Figure 14 shows snapshots of velocity vectors of wet particles ($e = 0.95$) with 1.0 wt % liquid, extracted from the midplane of the bed along the spanwise direction, when fluidizing velocities of 1.8 m s^{-1} and 2.8 m s^{-1} were applied. At a fluidizing velocity of 1.8 m s^{-1}, wet particles had the tendency to move as agglomerates, as indicated by the similar velocity vectors within a localized region. Such tendencies to move as agglomerates were reduced when the fluidizing velocity was increased to 2.8 m s^{-1}. The velocity vectors for jetsam particles near the bed bottom were larger for wet particles as compared to dry particles, as seen previously in Figure 7. Due to the increase in particle velocities when the amount of liquid present was 1.0 wt %, accumulation of jetsam particles at the bottom of the bed was greatly reduced, hence suppressing density segregation. As such, the maximum attainable Lacey index values increased from about 0.85 to 0.95 when the amount of liquid present was increased from 0.0 to 1.0 wt %. With the high tendencies for wet particles to move as agglomerates with similar velocities of the particles within each agglomerate, Figure 14 also shows that relative velocities between particles in contact were almost never greater than 1 m s^{-1} and this justifies the assumption of negligible viscous effects in comparison with surface tension effects of the capillary liquid bridge forces present and the model applied in this study.

Figure 15 shows the time evolution of average relative fluid drag forces ($\mathbf{f_{drag}/f_g}$) for wet flotsam and jetsam particles originally belonging to various zones within the fluidized bed for the different fluidizing velocities applied. In contrast to the profiles seen earlier for dry particles, there was a tendency for wet particles in different zones to exhibit synchronized fluctuations in drag forces during the fluidization process even for a fluidizing velocity of 1.8 m s^{-1}. Coupled with the tendency to form agglomerates, wet particles might then be expected to exhibit synchronized motions in the form of agglomerates, which would result in minimal density segregation. The

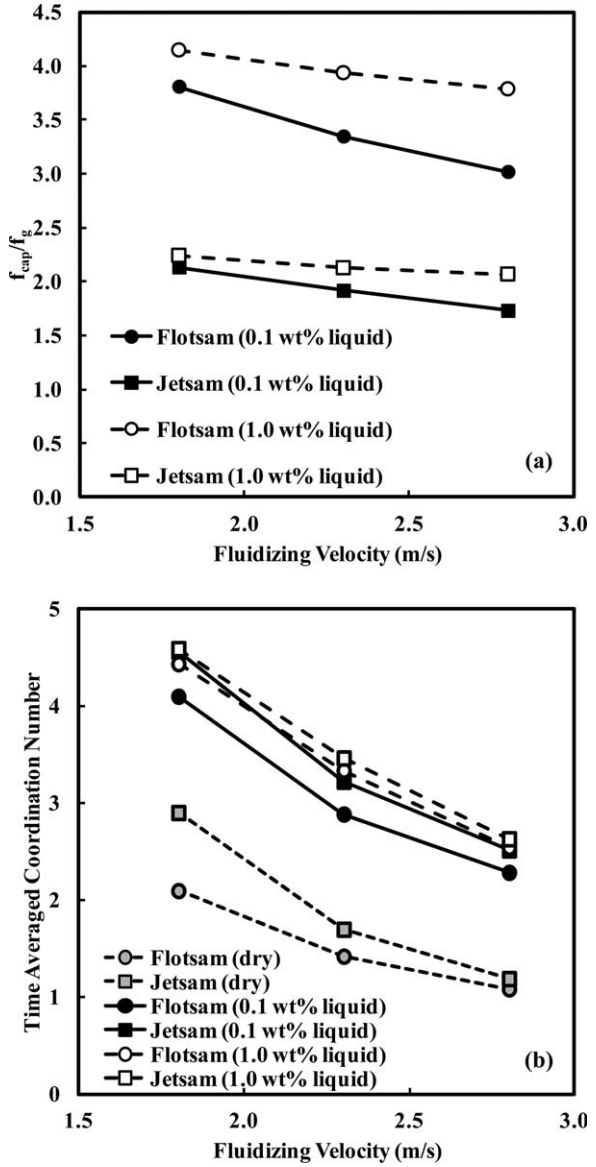

Figure 16. Effect of fluidizing velocity on (a) time-averaged relative capillary liquid bridge forces (f_{cap}/f_g) and (b) time-averaged coordination number for wet flotsam and jetsam particles ($e = 0.95$).

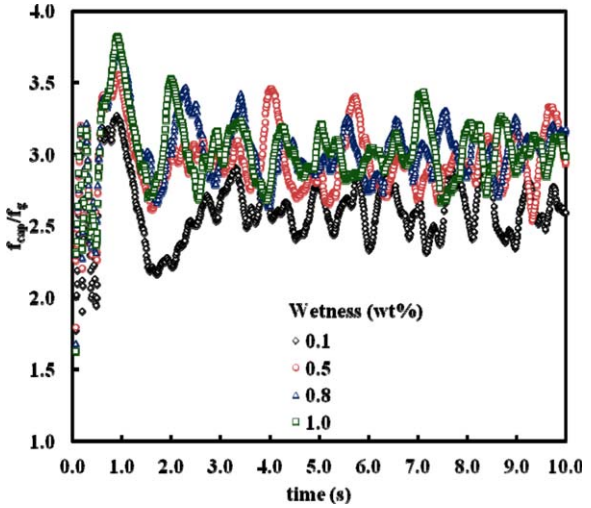

Figure 17. Time evolution of total capillary liquid bridge forces (f_{cap}/f_g) for different amounts of liquid present and fluidizing velocity of 2.3 m s^{-1}.

[Color figure can be viewed in the online issue, which is available at wileyonlinelibrary.com.]

synchronized fluctuations in drag forces also suggested that the bed had reached a macroscopically pseudosteady state, which explained why the Lacey index values seen earlier did not change much with time.

Figure 16a shows the effect of fluidizing velocity on time-averaged relative capillary liquid bridge forces for wet particles originally belonging to various zones within the fluidized bed. The magnitudes of relative capillary liquid bridge forces were observed to be higher for flotsam particles than for jetsam particles. This is a reflection of the fact that the weight of a flotsam particle is smaller than that of a jetsam particle while the total capillary liquid bridge forces experienced by both types of particles before nondimensionalization were similar. Figure 16b shows that the time-averaged coordination numbers of both wet flotsam and jetsam particles were similar at each fluidizing velocity. As the total capillary liquid bridge force experienced by a particle depended only on the number of nearest neighbors forming capillary liquid bridges with the particle, or equivalently the coordination number, this supported the previous statement that total capillary liquid bridge forces experienced by both wet flotsam and jetsam particles at each fluidizing velocity were similar. When the amount of liquid present between particles was simulated at 0.1 wt %, an increase in fluidizing velocity from 1.8 m s^{-1} to 2.8 m s^{-1} decreased the relative capillary forces acting on flotsam particles by approximately 21% (from 3.8 to 3.0) and the coordination number by approximately 44% (from 4.1 to 2.3). However, when the amount of liquid simulated was 1.0 wt %, the same increase in fluidizing velocity only decreased the relative capillary forces by approximately 8.5% (from 4.2 to 3.8) but the coordination number by approximately 43% (from 4.4 to 2.5). As the predominant effect of capillary forces was to cause agglomeration of wet particles, it might be expected that an increase in fluidizing velocity in a bed with a small amount (0.1 wt %) of liquid between particles would result in better mixing of particles while the same increase in fluidizing velocity would have minimal effect on mixing efficiency in a bed with a larger amount (1.0 wt %) of liquid. These behaviors were indeed observed earlier in the time evolution of Lacey index values for the various fluidized beds containing dry and wet particles.

Figure 17 shows the time variation of the total capillary liquid bridge forces (f_{cap}/f_g) for different amounts of liquid present in the bed when the fluidizing velocity was 2.3 m s^{-1}. The relative capillary forces acting on the particles fluctuated about 3.0 when the amounts of liquid simulated were 0.5 wt %, 0.8 wt %, and 1.0 wt %. This was only slightly higher than the relative capillary force of 2.5 when the amount of liquid present was 0.1 wt %. Although magnitudes of capillary liquid bridge forces did not vary significantly for the various amounts of liquid considered in this study, the formation of agglomerates by wet particles led to much reduced extents of density segregation. This was observed as more uniform mass fraction distributions of flotsam particles as well as higher Lacey index values for fluidized beds containing wet particles.

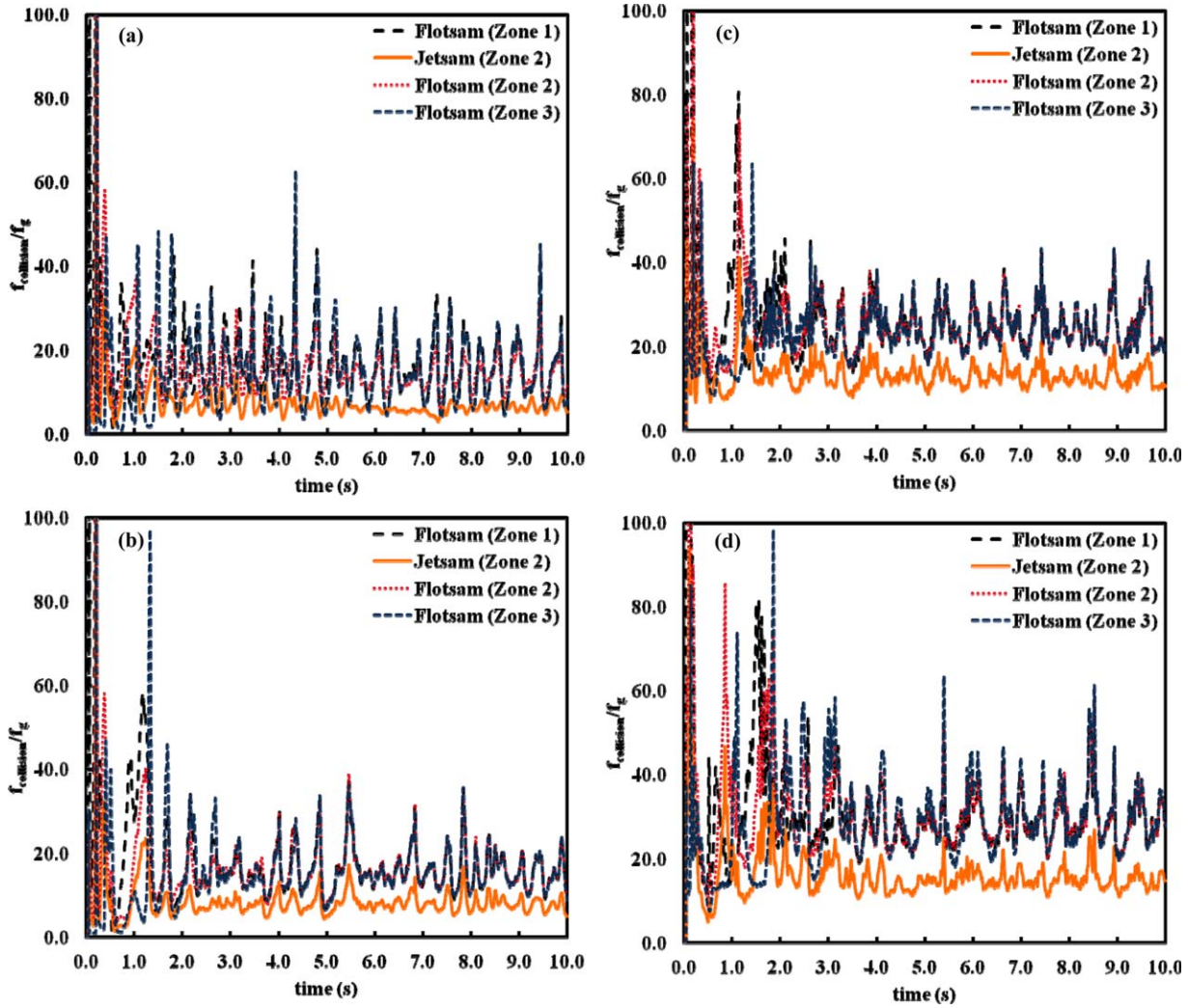

Figure 18. Time evolution of relative particle-particle collision forces ($f_{collision}/f_g$) for (a) dry particles with fluidizing velocity 1.8 m s^{-1}, (b) dry particles with fluidizing velocity 2.8 m s^{-1}, (c) wet particles with 1.0 wt % liquid and fluidizing velocity 1.8 m s^{-1} and (d) wet particles with 1.0 wt % liquid and fluidizing velocity 2.8 m s^{-1}.

[Color figure can be viewed in the online issue, which is available at wileyonlinelibrary.com.]

Figure 18 shows the time evolution of average relative collision forces ($f_{collision}/f_g$) for dry and wet flotsam and jetsam particles for the various fluidizing velocities applied. Here, collision force is defined as the sum of the contact and damping forces as defined in the linear spring-and-dashpot model. It may be seen that magnitudes of average collision forces were larger than those of capillary forces throughout the fluidization process. Furthermore, collision forces between particles increased with an increase in the fluidizing velocity applied. Thus, it might be expected that the basic condition required for mixing or segregation to occur, where collision forces overcome capillary forces acting between wet particles, was likely to be satisfied. In order for mixing or segregation to occur, the strong cohesive forces arising from capillary effects between wet particles would have to be overcome by particle-particle collision forces. This would then allow particles to be removed from one agglomerate to become an independent particle before joining another agglomerate. Such movements of particles between agglomerates were necessary for either mixing or segregation to occur during fluidization of wet particles. This explained the higher rate of density segregation and mixing observed in dry particles at low and high fluidizing velocities respectively in comparison with wet particles. Figure 18a shows that there were minimal fluctuations in collision forces for dry jetsam particles when a fluidizing velocity of 1.8 m s^{-1} was applied. One plausible reason for this was that the frequency of collisions for jetsam particles under these conditions was low due to segregation of jetsam particles at the bottom of the bed, thereby reducing fluctuations of collision forces in the system. Figure 18b shows that a higher fluidizing velocity of 2.8 m s^{-1} in a bed containing dry particles led to larger fluctuations in collision forces, hence resulting in a higher mixing efficiency, as observed earlier in the discussion on dry particle fluidization. Similarly, with the application of higher fluidizing velocities in beds containing wet particles (Figures 18c and d), larger fluctuations in particle-particle collision forces improved the likelihood of such forces overcoming capillary forces between wet particles and led to higher mixing efficiencies as seen earlier in the time evolution of Lacey index values for wet particles.

Conclusions

The mixing and segregation behaviors of dry and wet granular mixtures in gas fluidized beds were investigated computationally in this study. The conventional CFD-DEM model was coupled with a capillary liquid bridge force model and used for simulations of fluidization of dry and wet particles of different densities at various fluidizing velocities. The results obtained for fluidization of dry particles were in good agreement with previously reported Eulerian-Lagrangian simulation results. The degree of density segregation was found to decrease with increasing fluidizing velocities and coefficients of restitution. Sensitivity of the fluidized bed to the coefficient of restitution was also found to decrease when the coefficient of restitution increased from 0.95 to 0.99. An analysis of forces showed that magnitudes of drag forces acting on flotsam and jetsam particles were larger and smaller than their weights respectively. A lower tendency for density segregation was observed in fluidization of wet particles. Wet particles were fluidized as agglomerates with individual particles held together by capillary liquid bridge forces and exhibited synchronized motions as a result. These capillary liquid bridge forces between particles had to be overcome in order for mixing or segregation at the scale of individual particles to occur. Based on analyses of the time evolution of the various forces present during fluidization, it was observed that particle-particle collision forces were stronger than both fluid drag forces and capillary liquid bridge forces. The magnitudes of particle-particle collision forces and drag forces increased with increasing fluidizing velocity while the magnitudes of capillary forces decreased with increasing fluidizing velocity, which explained the higher mixing or segregation efficiencies observed in wet particles at higher fluidizing velocities. It is well recognized in the research literature that segregation of granular mixtures of particles with different sizes in gas fluidized beds, like density segregation, is a complex and incompletely understood phenomenon. It would thus be pertinent to extend the present study towards investigations of fluidization, mixing and segregation behaviors in fluidized beds containing dry or wet particles of different sizes.

Acknowledgments

This study has been supported by the National University of Singapore (NUS). The authors gratefully acknowledge the presentation of an Outstanding Undergraduate Dissertation/ Research Project Award by the AIChE Singapore Local Section for this study.

Literature Cited

1. Tardos G, Pfeffer R. Chemical reaction induced agglomeration and defluidization of fluidized beds. *Powder Tech.* 1995;85:29–35.
2. Wright PC, Raper JA. Role of liquid bridge forces in cohesive fluidization. *Chem Eng Res Design.* 1998;76:753–760.
3. Rhodes MJ, Wang XS, Nguyen M, Stewart P, Liffman K. Study of mixing in gas-fluidized beds using a DEM model. *Chem Eng Sci.* 2001;56:2859–2866.
4. McLaughlin LJ, Rhodes MJ. Prediction of fluidized bed behaviour in the presence of liquid bridges. *Powder Tech.* 2001;114:213–223.
5. Wormsbecker M, Pugsley T. The influence of moisture on the fluidization behaviour of porous pharmaceutical granule. *Chem Eng Sci.* 2008;63:4063–4069.
6. Halow J, Holsopple K, Crawshaw B, Daw S, Finney C. Observed mixing behavior of single particles in a bubbling fluidized bed of higher-density particles. *Ind Eng Chem Res* 2012;51:14566–14576.
7. Oshitani J, Kajimoto S, Yoshida M, Franks GV, Kubo Y, Nakatsukasa S. Continuous float-sink density separation of lump iron ore using a dry sand fluidized bed dense medium. *Adv Powder Technol.* 2013;24:468–472.
8. Oshitani J, Ohnishi M, Yoshida M, Franks GV, Kubo Y, Nakatsukasa S. Dry separation of particulate iron ore using density-segregation in a gas-solid fluidized bed. *Adv Powder Technol.* 2013; 24:554–559.
9. Cooper S, Coronella CJ. CFD simulations of particle mixing in a binary fluidized bed. *Powder Tech.* 2005;151:27–36.
10. Huilin L, Yunhua Z, Ding J, Gidaspow D, Wei L. Investigation of mixing/segregation of mixture particles in gas-solid fluidized beds. *Chem Eng Sci.* 2007;62:301–317.
11. Mikami T, Kamiya H, Horio M. Numerical simulation of cohesive powder behavior in a fluidized bed. *Chem Eng Sci.* 1998;53:1927–1940.
12. Darabi P, Pougatch K, Salcudean M, Grecov D. DEM investigations of fluidized beds in the presence of liquid coating. *Powder Tech.* 2011;214:365–374.
13. Lim EWC, Tan RBH, Xiao ZY. Mixing behaviors of wet granular materials in gas fluidized bed systems. *AIChE J.* 2013;59:4058–4067.
14. Liu PY, Yang RY, Yu AB. Self-diffusion of wet particles in rotating drums. *Phys Fluids.* 2013;25:063301.
15. Liu PY, Yang RY, Yu AB. The effect of liquids on radial segregation of granular mixtures in rotating drums. *Granular Matter.* 2013; 15:427–436.
16. Lim EWC. Pattern formation in vibrated beds of dry and wet granular materials. *Phys Fluids.* 2014;26:013301.
17. Lim EWC. Shear aggregation of colloidal nanoparticles. *J Chem Eng Jpn.* 2014;47:635–643.
18. Cundall PA, Strack ODL. A discrete numerical model for granular assemblies. *Geotechnique.* 1979;29:47–65.
19. Zhu HP, Zhou ZY, Yang RY, Yu AB. Discrete particle simulations of particulate systems: a review of major applications and findings. *Chem Eng Sci.* 2008;63:5728–5770.
20. Feng YQ, Yu AB. Assessment of model formulations in the discrete particle simulation of gas-solid flow. *Ind Eng Chem Res.* 2004;43: 8378–8390.
21. Di Felice R. The voidage function for fluid-particle interaction systems. *Int J Multiphase Flow.* 1994;20:153–159.
22. Ennis BJ, Li J, Tardos GI, Pfeffer R. The influence of viscosity on the strength of an axially strained pendular liquid bridge. *Chem Eng Sci.* 1990;45:3071–3088.
23. Feng YQ, Xu BH, Zhang SJ, Yu AB. Discrete particle simulation of gas fluidization of particle mixtures. *AIChE J.* 2004;50:1713–1728.
24. Feng YQ, Yu AB. Microdynamic modeling and analysis of the mixing and segregation of binary mixtures of particles in gas fluidization. *Chem Eng Sci.* 2007;62:256–268.
25. Lim EWC. Mixing behaviors of granular materials in gas fluidized beds with electrostatic effects. *Ind Eng Chem Res.* 2013;52:15863–15873.

Manuscript received Feb. 1, 2015, and revision received July 1, 2015.